Impact of the Bio Content of Polymeric Matrices on Flexural Performance of Sandwich Beams made of PET Fiber Composite Facings and Recycled PET Honeycomb Core

Raghad Kassab[1] and Pedram Sadeghian[2]

Department of Civil and Resource Engineering, Dalhousie University, 1360 Barrington St., Halifax, NS, B3H 4R2 Canada.

ABSTRACT:

This paper investigates the flexural performance of sandwich beams composed of polyethylene terephthalate (PET) fiber-reinforced polymer (FRP) composite facings and a recycled PET (R-PET) honeycomb core. The study aims to analyze the effects of different factors on the flexural performance of the sandwich beams, including the variation in bio content within the polymeric matrices, different facing thicknesses, and the orientation of the R-PET honeycomb core. Three different polymeric matrices, namely a synthetic resin, a partial bio-resin, and a bio-resin are considered. A total of 30 sandwich beam specimens (300mm long and 25mm wide) were prepared with three different facing thicknesses (1, 2, and 3mm) and two orientations of the R-PET honeycomb core (strong vs. weak axes) using the three polymeric matrices. The beam specimens were tested under four-point bending until failure. The facing and core materials were also tested in tension and shear, respectively, in two orthogonal directions. Significant non-linearity is observed in the behaviour of the beam specimens, which is rooted in the non-linearity of both facing and core materials. Additionally, the results demonstrate that alterations in polymer

[1] PhD Student, E-mail: r.kassab@dal.ca (corresponding author)

[2] Associate Professor and Canada Research Chair in Sustainable Infrastructure, E-mail: pedram.sadeghian@dal.ca

composition significantly impact the tensile properties of FRPs, which then affect the bending performance of the sandwich beams. To further corroborate experimental findings, a finite element simulation is also employed for analyzing the sandwich beams. The outcomes offer valuable insight for the designers planning to develop efficient and sustainable composite materials, thereby advancing the creation of environmentally friendly structural components.

KEYWORDS: Sustainability; Honeycomb; Recycled Plastic; PET; Bio-resin.

DOI: https://doi.org/10.1016/j.istruc.2023.105057

1. INTRODUCTION

Fiber-reinforced polymers (FRPs) have emerged as a versatile material in civil engineering, supported by numerous recent applications. They have been employed extensively in the rehabilitation of structural components, including bridges and buildings [1][2][3][4][5]. FRPs are also used as a facing component of sandwich panels [6], which are also known as structural insulated panels (SIPs) for commercial, residential, and institutional buildings [7][8][9][10][11]. Additionally, FRPs are increasingly employed for retrofitting of concrete structures to improve strength, ductility and energy dissipation capacity [12][13][14]. Moreover, FRPs are widely used for manufacturing underground components like pipelines in the oil and gas sector [15] and to fortify existing tunnels and substructures [16]. The widespread adoption of FRPs can be attributed to several key advantages, including a high strength-to-weight ratio [17], durability [18], moldability [19], and corrosion resistance [20]; they are an ideal choice for applications demanding a combination of strength and lightweight design [21].

Notable strength benefits of FRPs are accompanied and countered by significant environmental drawbacks. Specifically, the production process of conventionally utilized FRPs, including aramid FRP (AFRP), glass FRP (GFRP), and carbon FRP (CFRP), involves energy-

intensive fiber manufacturing [22]. Furthermore, using petroleum-derived epoxy in FRP production leads to the emission of greenhouse gases, which causes global warming alongside the accumulation of landfill waste and the release of toxic substances [23]. Given the significant negative environmental impact of FRP, it is crucial to prioritize measures that minimize resulting pollution. A vital step involves conducting a thorough evaluation of the production process for FRP components and identifying more sustainable alternative materials. By employing these approaches, the environmental footprint of FRPs can be significantly diminished, all the while satisfying the requirements of modern industries in a sustainable and efficient manner.

This research seeks to reduce the environmental impact of FRPs by exploring the use of polyethylene terephthalate (PET) fibers and bio-resins as substitutes for traditional fiber and polymer materials. Recently, an increase application of using PET fibers in FRP applications for seismic retrofitting has emerged [24][25][26][27]. Among these studies, the axial behaviour of PET FRP confined concrete circular and noncircular columns has been rigorously evaluated through experimental and numerical modelling techniques [28][29][30]. Tests conducted on FRP confined columns resulted in encouraging results, such as improved ductility, energy dissipation, and seismic performance of the confined column [24][25][26][27]. Furthermore, the maximum ultimate drift ratio increased by approximately 6 times due to confinement with PET FRPs [27].

Recently, research has emphasized not only identifying sustainable alternatives to conventional fiber materials, but also investigating sustainable options for the polymeric matrix component of FRPs. As a result, attention shifted towards using bio-resins derived from renewable resources as a replacement for traditional epoxy-based polymers [31][32][33][34][35]. This development could potentially further reduce the carbon footprint of FRPs and increase sustainability while still maintaining high-performance characteristics. Furthermore, fiber choice

affects overall strength, while the polymer component helps distribute the load and maintain fiber orientation [36]. Research conducted by Fam et al. [31] signified that a bio-resin GFRP composite achieved its maximum strength approximately 13 days after production. Nash et al. [33] also highlighted that the flexural strength of bio-epoxy laminates with 19% bio-content was comparable to epoxy laminates in dry conditions. Moreover, Hofmann et al. [34] tested a high-performance bio-based unsaturated polyester resin and compared it to a conventional petroleum-derived unsaturated polyester resin regarding mechanical and thermomechanical properties. Results indicated that the bio-based FRP composite exceeded the performance properties of its petroleum-derived counterpart, indicating potential for high-performance structural applications. Despite the promising findings, a significant research gap exists in determining the optimal combination of bio-resins and PET fibers for PET FRPs, as well as assessing their feasibility as sustainable alternatives to conventional synthetic polymers. To address this gap, the current study explores the impact of the bio content of polymeric matrices on the flexural performance of PET FRPs sandwich composites.

2. EXPERIMENTAL PROGRAM

The experiment involved testing three types of PET FRP materials: two with bio-resin and one with synthetic resin. Uniaxial tension tests were conducted on PET FRP coupons to assess the tensile properties of PET FRP, while four-point bending tests were performed on sandwich beams with PET FRP facings. Additionally, the core component was tested in shear to evaluate its shear stress-strain profile. The core was fabricated from a novel recycled PET material; it was necessary to determine its mechanical properties to create a model for verifying the bending test results.

2.1. Test Matrix

A total of 30 sandwich beams were divided into 10 sets, with each set comprised of three identical specimens underwent testing. The sets varied in several parameters, including: orientation of the honeycomb with respect to the sandwich beam length; the type of polymer used in both the FRP component; and the adhesive used to attach the facing and core components. Table 1 displays the testing matrix of the sandwich beams, where the specimen identification (ID) is comprised of three parts. The first ID part indicates the type of polymer used; "BE" denotes a combination of Epoxy and bio-resin with a bio-content of approximately 20% (partial bio-resin); "B" indicates furfuryl alcohol with approximately 100% bio-content (bio-resin), and "E" represents traditionally used non-bio-based epoxy (synthetic resin). The second ID part represents the thickness of the facing component; "ft" denotes the facing thickness, followed by an Arabic numeral. The final ID part is either "S"—representing a strong orientation of the core laid parallel to the length of the sandwich beams, or "W"—indicating a strong orientation of the core laid perpendicular to the length of the sandwich beams.

2.2. Material Properties

The fundamental mechanical properties of the three types of FRPs used in the sandwich sets were extracted through uniaxial tension tests, as shown in Figure 1, conducted in accordance with ASTM D882 [37]. The fabrication process was completed using a wet-layup technique, which involves several key steps. The fabric was first cut and measured. Subsequently, the resin and hardener were weighed to maintain the correct weight ratio. The initial layer of resin was then spread onto parchment paper. Next, two layers of PET fabric were stacked with the resin-hardener mixture sandwiched in between. The composite sheet was left to cure with weights placed on top

to remove excess resin during curing. The fabrication method was consistent for all coupons; the only differences were the type and ratio of resin and hardener used, and the curing time.

For the bio-resin PET FRP composite, Fam et al. [31] demonstrated that a mix of furfuryl alcohol (QuaCorr 1001) and 3% phthaloyl dichloride hardener (QuaCorr 2001) provided strength comparable to synthetic polymer-based FRPs. Therefore, this study adopted this resin-hardener ratio. As recommended by the manufacturer, the PET FRP composite made with epoxy and bio-content resin was fabricated using a 30% hardener component. Also, per manufacturer specifications, a recommended ratio of five parts epoxy to one part hardener was used for the epoxy PET FRP coupons. After mixing the resin and hardener, bio-resin had the most aggressive smell, while the other two resins had a similar, bearable smell.

Due to the moisture-sensitive nature of phthaloyl dichloride—a combination of phthaloyl chloride and dicarboxylic acid chloride—it readily hydrolyzes in the presence of moisture, liberating HCl. Furthermore, when phthaloyl dichloride is mixed with furfuryl alcohol, an exothermic polymerization reaction occurs, generating heat proportional to the number of reactants used. Thus, a fume hood ensured the safe handling and mixing of the bio-resin and hardener. Additionally, a mixing container was used, which had high thermal resistance compared to other resin types (e.g., synthetic resin and partial bio-resin). Environmental conditions, like moisture and air, were controlled before mixing. The bio-resin PET FRP composite had the longest curing time of 13 days, followed by the partial bio-resin resin PET FRP at seven days, and epoxy (synthetic resin) at the shortest, four days. Table 2 summarizes the key differences between the three matrix polymers: curing time, bio-content percentage, source of resin, and fabrication stage notes.

The PET FRP composite sheets were fully cured then cut into coupons for the uniaxial tension test. The bio-resin coupon was black—reflecting the color of furfuryl alcohol—while the

partial bio-resin coupons were light-colored (the latter bright and the former off-white). Additionally, curling was observed only in the PET FRP coupon made with bio-resin. This is attributed to increased water absorption of the bio-resin, which has a higher absorption rate due to its molecular structure, lower crosslinking density, and lower glass transition temperature (Tg) values compared to the epoxy matrix. The increased water absorption caused the PET FRP coupon to swell and warp, resulting in observed curling.

The coupons were subjected to uniaxial tension tests at a displacement-controlled loading condition of 2mm/minute, and the strain change was captured via strain extensometer. A data acquisition unit (DAQ) recorded the loading sustained by coupons, along with the change in strain data; it was captured at a rate of 10 data points per second. The test concluded when each coupon reached its ultimate load capacity or failed in tension. Next, the load data was converted to stress by dividing it by the cross-sectional area of the coupons, which were averaged from three locations on each coupon's cross-section. The coupons made with either synthetic resin or partial bio-resin had a similar stress-strain curve shape or bilinear trend. However, coupons made with bio-resin polymer had three distinct regions within the stress-strain curve, as illustrated in Figure 2 (c). The first showcased the greatest slope with a modulus of elasticity, E_1, of 5524 MPa and a standard deviation (SD) of 117.3 MPa (5524 ± 117.3 MPa) for longitudinal coupons and 4732 ± 497 for transverse coupons. The second depicted the least slope within a strain hardening region, with an average modulus "E_2" of 575 ± 84 for longitudinal coupons and 317 ± 50 MPa for transverse coupons. Furthermore, the third had an average modulus "E_3" of 1125 ± 25 MPa for longitudinal coupons and 649 MPa ± 85 for transverse coupons.

The stress response contrast between the longitudinal and transverse coupons varied according to the ratio of longitudinal-to-transverse PET fiber density, which is 2:1 as depicted in

Figure 2(a) and (b). The average ultimate strength, F_u, of the longitudinal coupons was determined to be 147 ± 17 MPa, 116 ± 11 MPa, and 117.3 ± 5 MPa for partial bio-resin, synthetic resin, and bio-resin polymer matrix, respectively. Similarly, the average ultimate strength of the transverse coupons was found to be 85 ± 3 MPa, 59 ± 7 MPa, and 65 ± 8 MPa for partial bio-resin, synthetic resin, and bio-resin polymer matrix, respectively. All coupons reached this strength at approximately the same ultimate strain, ε_u. A detailed summary of the main transition points and elasticity moduli, consistent with the regions indicated in Figure 2(c), can be found in Table 3 for longitudinal coupons and Table 4 for transverse coupons.

The shear properties of the R-PET honeycomb core were evaluated through rigorous testing conducted in accordance with ASTM C273 [38]. To determine the shear strength of the material, eight specimens were cut and affixed to steel plates using adhesive. Each specimen was 240mm long and 50mm wide, and 12mm thick. Four were oriented along the strong honeycomb direction, while the other four were oriented along the weak direction. Shear testing was performed using a shear test fixture, as depicted in Figure 3, and an Instron 8501 machine loaded the steel plates at a constant rate of 0.5mm/minute. The shear strain was not directly measured, but rather, calculated by dividing the measured separation distance of the two steel plates by the thickness of the sample core specimen. The load resisted by the specimens and the LP data were captured using a DAQ at a sampling rate of 10 data points per second. These load data were then used to calculate the shear stress. Specifically, the shear stress was computed by dividing the load resisted by the tested specimen by the interaction area - a product of the specimen's length and width (240mm and 50mm, respectively). Testing continued until each specimen reached its maximum load. Only specimens that exhibited diagonal tension shear failure were analyzed, excluding any other premature failure modes.

The results of the shear stress-strain analysis, as shown in Figure 4, revealed that both strong and weak honeycomb specimens exhibited similar shear stress-strain trends. The strong honeycomb specimens had an average shear modulus of approximately 80 ± 6 MPa, while weak specimens had a shear modulus of approximately 42 ± 6 MPa. The honeycomb specimens with strong orientation along the length of the steel plate fixture exhibited significantly higher strength capacity than those with weak orientation. Furthermore, the former exhibited an average strength capacity of 1.89 ± 0.05 MPa, and the latter had an average strength capacity of 0.79 ± 0.03 MPa.

2.3. Fabrication of Sandwich Beams

The sandwich beams were created using a multi-stage process. Initially, a piece of parchment paper was traced which guided the size and shape of the sandwich panel. The next step involved spreading the first resin layer on the parchment paper; this layer needed to be spread evenly to ensure uniform adherence of subsequent layers. Once prepared, the first fabric layer was placed, as indicated in Figure 5(a), which served as the first facing component of the sandwich panel. Since the honeycomb core component did not have any linings. Under typical circumstances, a lining would serve to prevent the resin from seeping into the honeycomb structure if it was applied to the top surface. However, in the absence of such a lining, a two-step fabrication process was adopted to prevent resin permeation into the honeycomb structure.

Following the placement of the initial facing layer, the unlined honeycomb core was positioned on top of the first fabric layer, as shown in Figure 5(b). Before advancing to the next stage, weights were placed on the first side of the sandwich beam. This step was crucial to ensure the layers adhered properly and the resin within the panel was evenly spread. The panel was then left to cure, solidifying the structure. After curing, the sandwich beams were cut from the panel, as shown in Figure 5(c). The resulting beams had a length of 250mm and a width of 75 mm.

Notably, the consistency of the panel source resulted in uniformity in the thickness of the individual beams. This is illustrated in Table 1, detailing the consistently maintained sample thickness across the sandwich beams. This process was performed on three sandwich panels, each with a different polymer matrix type within the PET FRP. Figure 5(d) shows a side view of the sandwich panel made with bio-resin. This resin resulted in curling due to its heightened water absorption capacity, causing the PET FRP sandwich to expand and distort. To analyze the effect of the honeycomb core direction, two sets of sandwich beams were cut from each panel. One set included beams that were cut perpendicular to the panel length, and the other set consisted of beams that were cut parallel to the panel length. This led to different honeycomb directions running parallel to the beam length in each set, resulting in variances in strength and performance.

2.4. Test Set-up

The experimental set-up consisted of placing a sandwich beam specimen on top of two steel surfaces—specifically designed to replicate the effect of rollers—to conduct four-point bending tests in accordance with ASTM C393 [39]. A controlled load was applied to the specimen at a displacement rate of 2mm per minute using the Instron testing machine. The load was then transferred from the Instron testing machine to two-point loads to emulate a four-point bending arrangement. All beams tested had a fixed distance of 36mm between the loading points, with an overhang distance of 25mm and an unsupported span length of 200mm. All beams tested had a fixed distance of 36mm between the loading points, with an overhang distance of 25mm and an unsupported span length of 200mm. Figure 6 depicts a schematic diagram of the set-up for the four-point bending test, along with a photograph captured during the test to provide visual clarity of its procedure. To measure the strain of the top and bottom surfaces during bending, two strain gauges were mounted on the mid-top and bottom points of the sandwich beam's facing component;

the readings were recorded. Additionally, the displacement at midspan—representative of the maximum displacement occurring at any point during bending—was measured using two LPs. This was achieved by placing a long steel piece on the midsection of the sandwich beam over the strain gauges. Two LPs were positioned against the edges of the steel plate to record displacement, and the resulting displacement was calculated by averaging the two LP readings. The strain gauges, LPs, and load cell were all connected to the DAQ, which captured 10 data points of each data type (strain, displacement, and load) per second.

3. RESULTS AND DISCUSSION

This section offers a comprehensive analysis of the experimental results obtained from testing sandwich beams under four-point bending conditions. Despite using a standardized testing methodology, the data revealed noticeable variations in key parameters across varying sets, including load-deflection, load-strain, and moment-curvature relationships. Additionally, a uniform failure mode was not observed among the tested beams. To elucidate these discrepancies, the following section provides an in-depth exploration of the unique failure mechanisms observed during the experiment.

3.1. Failure Mode

At peak load, three distinct failure modes were observed in sandwich beams subjected to bending. This section aims to explain the failure mode variations across three specific categories of test sets. The first category, detailed in Figure 7a, included sets with different polymer matrix compositions, as shown in Figure 7: Sets 1 and 4; Sets 7 and 8; and Sets 9 and 10. The transition in failure modes across these sets—from top face rupture in Sets 1 and 4 where synthetic resin was used, to bottom face rupture in Set 7 and top face rupture in Set 8 with partial bio-resin, culminating in core shear failure in Sets 9 and 10 with bio-resin—can be attributed to the type of polymer

matrix used. For beams where epoxy or partial synthetic resin was employed, the strength of the facing was adequate to withstand tensile compression stresses, preventing significant core displacement and thereby averting core shear failure. Instead, these beams exhibited facing rupture. The change from top face to bottom face rupture was not significant as the stresses on both faces should be approximately the same. Notably, the use of bio-resin led to larger beam displacements compared to partial bio-resin or synthetic resin, which resulted in core shear due to these large displacements.

The second category, shown in Figure 7b, comprises test sets using identical polymer matrices and component types but features different honeycomb orientations. This group includes Sets 1, 2, 3, 7, 9 and Sets 4, 5, 6, 8, 10. Altering honeycomb orientation had minimal impact on the sandwich beams' failure mechanisms, with no significant change in failure mode for beams made from the same material and different honeycomb orientations. The lone exception was noted in the epoxy polymer matrix, where a slight change in failure mode was observed—from bottom face tensile rupture in Set 7 to top face compression rupture in Set 8. However, this change was minimal given the close proximity of tensile stresses in the top and bottom faces.

The final category, illustrated in Figure 7c, includes test sets with the same partial bio-resin polymer matrix, but with varying thicknesses of facing components (i.e., Sets 1 and 4, Sets 2 and 5, and Sets 3 and 6). For these, variations in face thickness led to changes in the failure mode of the sandwich beam, transitioning from face rupture in Sets 1 and 4 (with one mm-thick facing components) to core shear in Sets 2, 3, 5, and 6 (with 2 mm and 3 mm thick facing components). This shift in failure mechanisms is attributed to the increased strength and reduced vulnerability to failure of the thicker-facing components. In turn, causing the core to become the weaker element and govern failure mode.

3.2. Load-deflection

The load sustained by each sandwich beam was plotted against the midspan deflection at each load step, with increments of 10 data points per second and a loading rate of 2mm per minute; Figure 8 displays the resulting load-deflection plots. As illustrated in Figure 8(a) and (b), the variation in polymer components directly influences the overall load-deflection relationship of sandwich beams. This effect is notably pronounced for sandwich beams of strong honeycomb orientation, as seen in Figure 8(a).

For sandwich beams with strong honeycomb orientation along the length, the sets created using a partial bio-resin polymer matrix exhibited the highest ultimate load, averaging 1.6 kN. These were the only beams that displayed a linear load-displacement relationship to the failure point, a characteristic determined from the initial linear section of their load-displacement curve. Stiffness, quantified in N/mm, was obtained by determining the slope of this initial linear region of the load-displacement curve. This was computed using the ratio of change in load (in N) to the corresponding change in displacement (in mm) during the linear region, before the yielding point. Conversely, when the polymer component shifted from partial bio-resin to either synthetic resin or bio-resin, the load-deflection relationship appeared as a bilinear curve. Beams made of synthetic resin reached an average ultimate load of 1.4 kN, while those with bio-resin polymer achieved an average ultimate strength of approximately 1.5 kN. Significantly, the initial linear trend of these specimens had a similar slope (stiffness) to those made with partial bio-resin polymer—around 200 N/mm.

Although the sandwich beam set made with synthetic resin and the set made with bio-resin demonstrated comparable ultimate load capacities and a bilinear load-deflection pattern, the load-deflection relationships displayed notable differences, as illustrated in Figure 8(a). Distinctly, the

synthetic resin samples exhibited a secondary linear trend with an average stiffness, of 33.7 N/mm, occurring at a higher average load of 950 N. The second trend experienced fluctuations; the stiffness dropped and recovered until it reached failure point, potentially due to honeycomb cracking until achieving the ultimate strength of the bottom face. Regardless, the bio-resin polymer-based samples reached the secondary linear load-deflection trend at a lower average load of 460 N. This trend remained consistent and smooth up to the failure point, without fluctuations, and exhibited an average secondary stiffness of 42.7 N/mm.

For sandwich beams constructed from identical facing material (PET FRP with partial bio-resin) and core material (R-PET honeycomb), a nearly bi-linear load deflection pattern was observed when facing thickness varied, as shown in Figure 8(c). Furthermore, the initial beam stiffness increased proportionally with the growth in facing thickness. For beams with strong honeycomb orientation along their length, the average initial stiffness shifted from 210.8 N/mm for those with a facing thickness of approximately 1mm; to an average of 318 N/mm for those with a facing thickness of approximately 2mm; then to an average of 493.9 N/mm for beams with a facing thickness of approximately 3mm.

Following the analysis of the strongly oriented R-PET core, the investigation realigned to the weakly oriented R-PET core. As shown in Figure 8(d), sandwich beams with weakly oriented R-PET cores and partial bio-resin matrices were studied with varied PET FRP thicknesses; Sets 4, 5, and 6 were evaluated in this context. Interestingly, a similar pattern to that displayed in the strongly oriented samples was observed. The load-deflection relationship also appeared to follow a nearly bi-linear pattern when facing thickness varied. The initial beam stiffness also increased proportionally with the growth in facing thickness. However, the stiffness values were generally lower than those of strongly oriented beams, likely due to the different orientations of the

honeycomb core, which might have affected strength and stiffness. A comprehensive analysis of the load-displacement curves for all tested beams is provided in tabular form. Table 5 displays data for sandwich beams made with partial bio-resin polymer; Table 6 for those made exclusively with epoxy polymer; and Table 7 for sandwich beams made with bio-resin polymer. Table 8 details sandwich beams with weakly oriented R-PET core and partial bio-resin matrices. The analysis encompasses the initial stiffness (K_1), ultimate load (F_u) and displacement (δ_u).

3.3. Load-strain

Both the force exerted and the deformation in central regions of the composite beams was carefully monitored throughout flexural analysis. Furthermore, PET FRP demonstrated significant deformation capabilities consistent with findings from the previous section. Due to the high degree of deformation, the data generated from the flexural analysis occasionally exceeded the strain gauges' evaluation range—except during the initial stages before PET FRP underwent plastic deformation. Figure 9 presents the load-strain diagrams for all assessed sandwich beams.

During the initial phase of the flexural analysis—as depicted in Figure 9(a)—the load-strain response was consistent across all beam groups composed of various polymer types and identical dimensions. However, sandwich beams constructed with bio-resin polymer began deviating from the load-strain trend observed in other groups, experiencing greater strain at a given load (specifically, when a load of approximately 450N was reached). This is consistent with the observation that PET FRP coupons made with bio-resin polymer exhibit a larger strain change at a given stress once the yield stress was reached, as demonstrated in Figure 2, compared to PET FRP coupons made with epoxy polymer or a combination of partial bio-resin polymer.

Regarding the load-strain relationship for sandwich beams constructed using partial bio-resin polymer with varying facing thicknesses, the strain change exhibits an inverse proportionality

with the increase in facing thickness. This can be primarily attributed to when the facing component of the sandwich beam thickens, the overall stiffness increases, deeming it less prone to deflection under a given load. Consequently, the facing component experiences reduced strain at a given load, as demonstrated in Figure 9(b). As shown in Figure 9(c), for sandwich beams with a strongly oriented R-PET core and partial bio-resin matrices, the load-strain relationship also changed with varying facing thicknesses. Similar to the trends observed in Figure 9(b), an increase in facing thickness led to reduced strain at a given load due to increased overall stiffness.

Lastly, the sandwich beams with weakly oriented R-PET cores and partial bio-resin matrices displayed a similar trend, as shown in Figure 9(d). However, due to the weaker orientation of the core, these beams exhibited slightly higher strains compared to their strongly oriented counterparts with the same facing thickness. This suggests the orientation of the honeycomb core plays a crucial role in the load-strain relationship of these sandwich beams.

3.4. Moment-curvature

The sandwich beam's moment-curvature relationship was established by analyzing the changes in load and strain during the four-point bending test, which allowed an examination of beam ductility in the test matrix. The moment resistance value of the sandwich beams in the area between the two-point loads was determined from the load employed in the experimental evaluation. Simultaneously, beam curvature was calculated by dividing the difference between the top strain (compression strain) and the bottom strain (tension strain), obtained from the top and bottom surfaces of the sandwich beams, by the thickness (total depth) of the core component. This can be expressed by the following equation:

$$\text{Curvature} = \frac{\text{Compression Strain} - \text{Tension Strain}}{\text{Total depth}} \qquad [1]$$

The moment-curvature relationship for all tested sandwich beams is shown in Figure 10. Figures 10(b) and (d) emphasize that the facing component thickness is the most crucial factor impacting the beams' curvature extent. Specifically, a sandwich beam with a thicker facing component displays increased stiffness, leading to a higher resistance to curvature for a given moment. In contrast, Figures 10(a) and (c) illustrate that changes in the polymer component of the sandwich beams' facing material do not result in significant alterations to the moment-curvature relationship.

4. NUMERICAL INVESTIGATIONS

This section presents a Finite Element (FE) analysis, focusing on simulating the behaviour of sandwich beams under four-point bending configuration. The model—developed with SolidWorks Software—effectively generates load-strain, moment-curvature, and load-displacement data while considering both material and geometric nonlinearities through a systematic, iterative cross-sectional evaluation. The primary objective of this simulation was to validate the experimental results, which were duly confirmed through analysis.

4.1. Model Overview

The FE model employs finite element analysis to examine the behaviour of sandwich beams under bending. This investigation explores the impact of variable facing thicknesses (1, 2, and 3mm) for sandwich beams fabricated using partial bio-resin polymer matrix. Additionally, the study assesses the effect of different polymer matrix types on beams with a 1mm facing thickness. All beams exhibit a consistent core thickness of 12mm and honeycomb core orientations in both weak and strong directions. The four-point bending set-up was employed to establish boundary conditions, encompassing both supports and applied loads. Material properties were characterized by a nonlinear stress-strain relationship for the facing component, which was derived from coupon

testing of PET FRP and various bio-resin types. Material properties for the core, defined by linear stress-strain relationships illustrated in Figure 4, were sourced from the experimental coupon testing of R-PET honeycomb conducted in both the strong and weak honeycomb directions. These experimentally determined properties were then applied to the solid core model within SolidWorks, thus accurately representing the core's behavior within the simulations.

The stiffness matrix is crucial in finite element analysis, illustrating the connection between displacements at nodes and the forces exerted on a structure. For sandwich beams, the stiffness matrix is formed by integrating the stiffness contributions from individual elements throughout the entire structure. The Newton-Raphson method, an effective iterative numerical technique for solving nonlinear equations, was applied in this analysis. This method was used to determine the root of the nonlinear load-deflection, moment-curvature, and load-strain equations, which describe the sandwich beam's mechanical response under four-point bending. The process was refined iteratively until the difference between successive estimates fell below a pre-established tolerance level of 0.001. A high-quality solid mesh was generated using the blended curvature-based mesher, consisting a total of 112,137 nodes. The aspect ratio metrics depicted that 0% of elements had an aspect ratio greater than 10, and 4.31% of elements had an aspect ratio less than three The integration of the Newton-Raphson method and the stiffness matrix within the SolidWorks FEA enabled a more comprehensive understanding of the sandwich beams' performance, establishing a solid basis for advanced exploration and optimization of the sandwich beam's mechanical response characteristics under various loading conditions.

4.2. Model Verification

Detailed in Section 3, the experimental results were employed to validate the proposed FE model, which examined the behaviour of five distinct sandwich beams. Each of these beams

comprised a R-PET honeycomb core with PET FRP facings. The mechanical properties of PET FRP, which formed the top and bottom-facing components of the sandwich beams, were assumed to be consistent in tension and compression. This assumption was predicated on the observation that numerous materials exhibit analogous mechanical properties in tension and compression. Due to practical constraints, only tensile tests were conducted on the PET FRP coupons. The strain of PET FRP facing was analyzed using strain gauges located at the mid-span of the sandwich beams in both tension and compression facings. This comparison between the model and the experimental data indicated that the load-strain relationship derived from the simulation was more precise for the tension side (the bottom-facing component of the sandwich beam) than the negative strain reading in the top-facing component. In all cases, the model accurately predicted the stiffness of the experimental curves, indicating a strong correlation between the simulated and experimental results.

5. CONCLUSIONS

This paper investigated the effects of different polymer types on the performance of sandwich beam structures. Three polymers, specifically a synthetic epoxy resin and two bio-based resins, were examined as matrices in the FRP facings and as adhesive elements between the facing and core components. The analysis began with an assessment of the tensile behavior and ultimate strength of FRP composite coupons, fabricated using a consistent fiber material but varying polymer matrices under uniaxial tension. The elastic tension modulus and stress-strain profiles for each coupon were reported. Subsequently, the FRP composites were incorporated into the facing components of sandwich beams, all of which feature a recycled polyethylene terephthalate (R-PET) honeycomb core with a density of 100 kg/m^3 and a thickness of 12mm. The facing thicknesses range from 1mm to 3mm across the beam sets. The sandwich beams were tested under

bending. A finite element model was also developed and validated using the experimental results. The following conclusions can be determined:

- The polymer composition affects both the tensile and bending properties of FRPs and sandwich panels. Bio-resin polymers show a unique triphasic stress-strain curve, different from the bilinear trends in partial bio-resin and synthetic resin polymers. Sandwich beams with partial bio-resin reached an ultimate load of 1.6 kN, 14% higher than synthetic resin beams (1.4 kN), and 7% higher than bio-resin beams (1.5 kN). Thus, the careful choice of polymer matrix can improve the performance of composite structures by up to 14%.
- The study underscores that the type of polymer matrix, thickness of facing components, and honeycomb orientation are pivotal in defining the failure modes of sandwich beams. Changing from synthetic to bio-resin polymer matrix causes a transition in failure modes from either top or bottom face rupture to core shear. A similar shift from face rupture to core shear is observed when the thickness of the facing components is increased. On the contrary, alterations in honeycomb orientation have shown minimal effects on the failure mode. Use of bio-resin may lead to larger displacements, resulting in core shear failure that could require design adjustments.
- The beams comprised of partial bio-resin polymer matrix exhibited the highest ultimate load, which represents a 14% increase compared to beams made of the synthetic resin and a 7% increase compared to those with bio-resin.
- The initial beam stiffness increased proportionally with the increase in facing thickness. Beams with a facing thickness of approximately 2mm had an average initial stiffness of 51% higher than those with a facing thickness of approximately 1mm. Similarly, beams with a facing

thickness of approximately 3mm had an average initial stiffness of 55% higher than those with a facing thickness of approximately 2mm.

- The orientation of the honeycomb core exhibited a marginal influence on the stiffness of the composite sandwich beams. A variation of approximately 5% in initial stiffness was observed when the honeycomb core's orientation shifted from strong to weak. Nonetheless, the primary determinant of the sandwich beams' mechanical performance—encompassing load-deflection, load-strain, and moment-curvature relationships—was identified as the polymer matrix composition.
- The FE model was effective in simulating the load-displacement behaviour of the sandwich beams under four-point bending. The model provided valuable insight into the sandwich beams' mechanical response and successfully validated the experimental results, demonstrating a strong correlation between the simulated and experimental data.

6. ACKNOWLEDGEMENT

The authors acknowledge Dr. Jochen Pflug, Wouter Winant, and Friedrich Zerling of ThemHex and EconCore for supplying the R-PET honeycomb core. Additionally, the authors express appreciation to Dr. Michael McGeary and Pennakem for providing the bio-resin and offering expert guidance on safe handling throughout the project.

7. DATA AVAILABILITY

The raw/processed data required to reproduce these findings cannot be shared at this time due to technical or time limitations.

8. REFERENCES

[1] Valluzzi MR, Modena C, de Felice G. Current Practice and Open Issues in Strengthening Historical Buildings With Composites. Materials and Structures. 2014;47(12):1971-1985. doi:10.1617/s11527-014-0359-7.

[2] Mara V, Haghani R, Harryson P. Bridge Decks of Fibre Reinforced Polymer (FRP): A Sustainable Solution. Construction and Building Materials. 2014;50:190-199. doi:10.1016/j.conbuildmat.2013.09.036.

[3] Li M, Shen D, Yang Q, Cao X, Liu C, Kang J. Rehabilitation of Seismic-Damaged Reinforced Concrete Beam-Column Joints With Different Corrosion Rates Using Basalt Fiber-Reinforced Polymer Sheets. Composite Structures. 2022;289:115397. doi:10.1016/j.compstruct.2022.115397.

[4] Bakis CE, Bank LC, Brown V, Cosenza E, Davalos JF, Lesko JJ, Machida A, Rizkalla SH, Triantafillou TC. Fiber-reinforced polymer composites for construction—State-of-the-art review. Journal of composites for construction. 2002 May;6(2):73-87. doi: 10.1061/(ASCE)1090-0268(2002)6:2(73).

[5] Zoghi M, editor. The international handbook of FRP composites in civil engineering. CRC Press; 2013 Sep 26.

[6] Balıkoğlu, F., Demircioğlu, T. K., & Ataş, A. (2022). An experimental study on the flexural behaviour of symmetric and asymmetric marine composite sandwich beams. Journal of Composite Materials, 56(15), 2311–2325. https://doi.org/10.1177/00219983221089713.

[7] Mohamed M, Hussein R, Abutunis A, Huo Z, Chandrashekhara K, Sneed LH. Manufacturing and evaluation of polyurethane composite structural insulated panels.

Journal of Sandwich Structures & Materials. 2016;18(6):769-789. doi:10.1177/1099636215626597.

[8] Jacques E, Makar J. Behavior of structural insulated panels subjected to short-term axial loads. Journal of Structural Engineering. 2019;145(11). doi:10.1061/(asce)st.1943-541x.0002393.

[9] Mugahed Amran YH, El-Zeadani M, Huei Lee Y, Yong Lee Y, Murali G, Feduik R. Design innovation, efficiency and applications of structural insulated panels: A Review. Structures. 2020;27:1358-1379. doi:10.1016/j.istruc.2020.07.044.

[10] Fam A, Sharaf T, Sadeghian P. Fiber element model of sandwich panels with soft cores and composite skins in bending considering large shear deformations and localized skin wrinkling. Journal of Engineering Mechanics. 2016 May 1;142(5):04016015. doi: 10.1061/(ASCE)EM.1943-7889.0001062.

[11] MacDonnell L, Sadeghian P. Experimental and analytical behaviour of sandwich composites with glass fiber-reinforced polymer facings and layered fiber mat cores. Journal of Composite Materials. 2020 Dec;54(30):4875-87. doi: 10.1177/0021998320939625.

[12] Choi D, Hong S, Lim M-K, Ha S-S, Vachirapanyakun S. Seismic Retrofitting of Reinforced Concrete Circular Columns using Carbon Fiber, Glass Fiber, or Ductile PET Fiber. International Journal of Concrete Structures and Materials. 2021;15(1). doi:10.1186/s40069-021-00484-7.

[13] Yooprasertchai E, Wiwatrojanagul P, Pimanmas A. Using Natural Sisal and Jute Fiber Composites for Seismic Retrofitting of Nonductile Rectangular Reinforced Concrete

Columns. Journal of Building Engineering. 2022;52:104521. doi:10.1016/j.jobe.2022.104521.

[14] Sadeghian P, Rahai AR, Ehsani MR. Experimental study of rectangular RC columns strengthened with CFRP composites under eccentric loading. Journal of Composites for Construction. 2010 Aug;14(4):443-50. doi:10.1061/(ASCE)CC.1943-5614.0000100

[15] Alabtah FG, Mahdi E, Eliyan FF. The use of fiber reinforced polymeric composites in pipelines: A Review. Composite Structures. 2021;276:114595. doi:10.1016/j.compstruct.2021.114595

[16] Liu D, Shang Q, Li M, Zuo J, Gao Y, Xu F. Cracking behavior of tunnel lining reinforced with FRP grid-PCM method under bias pressure. Tunnelling and Underground Space Technology. 2022;123:104436. doi:10.1016/j.tust.2022.104436.

[17] Cui W, Fernando D, Heitzmann M, Gattas JM. Manufacture and structural performance of modular hybrid FRP-timber thin-walled columns. Composite Structures. 2021;260:113506. doi:10.1016/j.compstruct.2020.113506.

[18] Duo Y, Liu X, Liu Y, Tafsirojjaman T, Sabbrojjaman M. Environmental impact on the durability of FRP reinforcing bars. Journal of Building Engineering. 2021;43:102909. doi:10.1016/j.jobe.2021.102909.

[19] Berardi VP, Perrella M, Armentani E, Cricrì G. Experimental investigation and numerical modeling of creep response of glass fiber reinforced polymer composites. Fatigue & Fracture of Engineering Materials & Structures. 2021;44(4):1085-1095. doi:10.1111/ffe.13415.

[20] Tharmarajah G, Taylor SE, Cleland DJ, Robinson D. Corrosion-resistant FRP reinforcement for bridge deck slabs. Proceedings of the Institution of Civil Engineers - Bridge Engineering. 2015;168(3):208-217. doi:10.1680/jbren.13.00001.

[21] Mugahed Amran YH, Alyousef R, Rashid RSM, Alabduljabbar H, Hung C-C. Properties and Applications of FRP in Strengthening RC Structures: A Review. Structures. 2018;16:208-238. doi:10.1016/j.istruc.2018.09.008.

[22] Wang B, Bachtiar EV, Yan L, Kasal B, Fiore V. Flax, basalt, E-glass FRP and their hybrid FRP strengthened wood beams: An experimental study. Polymers. 2019;11(8):1255. doi:10.3390/polym11081255.

[23] Ead AS, Appel R, Alex N, Ayranci C, Carey JP. Life Cycle Analysis for green composites: A review of literature including considerations for local and global agricultural use. Journal of Engineered Fibers and Fabrics. 2021;16:155892502110269. doi:10.1177/15589250211026940.

[24] Dai J-G, Lam L, Ueda T. Seismic retrofit of square RC columns with Polyethylene Terephthalate (PET) fibre reinforced polymer composites. Construction and Building Materials. 2012;27(1):206-217. doi:10.1016/j.conbuildmat.2011.07.058.

[25] Zhou Y, Chen X, Wang X, Sui L, Huang X, Guo M, Hu B. Seismic Performance of large rupture strain FRP retrofitted RC columns with Corroded Steel Reinforcement. Engineering Structures. 2020;216:110744. doi:10.1016/j.engstruct.2020.110744.

[26] Sui L, Liu Y, Zhu Z, Hu B, Chen C, Zhou Y. Seismic Performance of LRS-FRP–Concrete–steel tubular double coupling beam. Applied Sciences. 2021;11(5):2024. doi:10.3390/app11052024.

[27] Mei S-J, Bai Y-L, Dai J-G, Han Q. Seismic behaviour of shear critical square RC columns strengthened by large rupture strain FRP. Engineering Structures. 2023;280:115679. doi:10.1016/j.engstruct.2023.115679.

[28] Saleem S, Pimanmas A, Qureshi MI, Rattanapitikon W. Axial behavior of pet frp-confined reinforced concrete. Journal of Composites for Construction. 2021;25(1). doi:10.1061/(asce)cc.1943-5614.0001092.

[29] Zhou J-K, Lin W-K, Guo S-X, Zeng J-J, Bai Y-L. Behavior of FRP-confined FRP spiral reinforced concrete square columns (FCFRSCs) under axial compression. Journal of Building Engineering. 2022;45:103452. doi:10.1016/j.jobe.2021.103452.

[30] Saleem S, Hussain Q, Pimanmas A. Compressive behavior of PET FRP–confined circular, square, and rectangular concrete columns. Journal of Composites for Construction. 2017;21(3). doi:10.1061/(asce)cc.1943-5614.0000754.

[31] Fam A, Eldridge A, Misra M. Mechanical characteristics of glass fibre reinforced polymer made of furfuryl alcohol bio-resin. Materials and Structures. 2013;47(7):1195-1204. doi:10.1617/s11527-013-0122-5.

[32] Tomlinson D, Fam A. Axial response of flax fibre reinforced polymer-skinned tubes with lightweight foam cores and bioresin blend. Thin-Walled Structures. 2020;155:106923. doi:10.1016/j.tws.2020.106923.

[33] Nash N, Egan L, Bachour C, Manolakis I, Comer A. Bio-based epoxy resin systems as potential alternatives to petroleum based epoxy matrices in marine fibre-reinforced polymer composites. Open Access Repository of the FIBRESHIP project. 2019. Available from: https://www.scipedia.com/public/Nash_et_al_2019a.

[34] Hofmann M, Shahid AT, Machado M, Garrido M, Bordado JC, Correia JR. GFRP biocomposites produced with a novel high-performance bio-based unsaturated polyester resin. Composites Part A: Applied Science and Manufacturing. 2022;161:107098. doi:10.1016/j.compositesa.2022.107098.

[35] Gabriel S, Langdon GS, von Klemperer CJ, Kim Yuen SC. Blast behaviour of fibre reinforced polymers containing sustainable constituents. Journal of Reinforced Plastics and Composites. 2022;41(19-20):771-790. doi:10.1177/07316844211072529.

[36] Uddin N. Developments in Fiber-Reinforced Polymer (Frp) Composites for Civil Engineering. Woodhead Publishing Limited; 2013.

[37] ASTM. (2018). ASTM D882, Standard Test Method for Tensile Properties of Thin Plastic Sheeting. ASTM. West Conshohocken, Pennsylvania, United States

[38] ASTM. (2020). ASTM C273, Standard Test Method for Shear Properties of Sandwich Core Materials. ASTM. West Conshohocken, Pennsylvania, United States.

[39] ASTM. (2020). ASTM C393, Standard Test Method for Core Shear Properties of Sandwich Constructions by Beam Flexure. ASTM. West Conshohocken, Pennsylvania, United States.

Table 1. Test Matrix of Sandwich Beams

Set #	Specimen ID	Facing Thickness "t_f" (mm)	Sandwich Beam Sample Thickness (mm)	Honeycomb Core Orientation	Polymer Type	Number of Specimens
1	BE-ft1-S	1	14	Strong	Partial Bio-Resin	3
2	BE-ft2-S	2	16	Strong	Partial Bio-Resin	3
3	BE-ft3-S	3	18	Strong	Partial Bio-Resin	3
4	BE-ft1-W	1	14	Weak	Partial Bio-Resin	3
5	BE-ft2-W	2	16	Weak	Partial Bio-Resin	3
6	BE-ft3-W	3	18	Weak	Partial Bio-Resin	3
7	E-ft1-S	1	14	Strong	Synthetic Resin	3
8	E-ft1-W	1	14	Weak	Synthetic Resin	3
9	B-ft1-S	1	14	Strong	Bio-resin	3
10	B-ft1-W	1	14	Weak	Bio-resin	3
Total						30

Table 2. Matrix Polymer Comparison for PET FRP Composite

Polymer Matrix	Bio Content (%)	Curing Time (Days)	Source of Resin	Fabrication Phase
Synthetic Resin	0	4	Petroleum based	Requires rapid processing
Partial Bio-Resin	20	7	Plant, Petroleum	Requires rapid processing
Bio-Resin	100	13	Waste by-products	Requires fume hood

Table 3. Summary of longitudinal tensile test results for PET FRP

Coupon ID		E_1 (MPa)	E_2 (MPa)	E_3 (MPa)	ε_y (mm/mm)	F_y (MPa)	ε_h (mm/mm)	F_h (MPa)	ε_u (mm/mm)	F_u (MPa)
PET FRP-BE	**Average**	4705	1544		0.0075	35.0			0.0815	147.0
	SD	909	23		0.0013	8.1			0.0065	16.6
PET FRP-E	**Average**	3305	1137		0.0068	23.2			0.0924	116.0
	SD	42	91		0.0016	5.6			0.0164	11.4
PET FRP-B	**Average**	5224	575	1125	0.0073	29.9	0.0353	48.1	0.1023	117.3
	SD	550	84	25	0.0003	5.8	0.0038	2.6	0.0042	4.6

Footnote: *Empty cells in the table correspond to coupons made with synthetic resin and coupons made with partial bio-resin. These coupons exhibit a bi-linear stress-strain relationship, and as such, only initial and final modulus and stress values are provided. In contrast, coupons made with bio-resin undergo three stages and possess a trilinear stress-strain relationship, which is why all cells are filled in for those coupons.

Table 4. Summary of transverse tensile test results for PET FRP

Coupon ID		E_1 (MPa)	E_2 (MPa)	E_3 (MPa)	ε_y (mm/mm)	F_y (MPa)	ε_h (mm/mm)	F_h (MPa)	ε_u (mm/mm)	F_u (MPa)
PET FRP-BE	**Average**	4167	806		0.0081	34.1			0.0712	85.5
	SD	22	33		0.0003	1.3			0.0050	3.3
PET FRP-E	**Average**	2345	606		0.0073	17.6			0.0769	58.8
	SD	215	90		0.0006	0.9			0.0023	6.5
PET FRP-B	**Average**	4732	317	649	0.0063	18.5	0.0315	26.6	0.0943	65.0
	SD	497	50	85	0.0012	0.6	0.0057	2.5	0.0051	8.3

Footnote: *Empty cells in the table correspond to coupons made with synthetic resin and coupons made with partial bio-resin. These coupons exhibit a bi-linear stress-strain relationship, and as such, only initial and final modulus and stress values are provided. In contrast, coupons made with bio-resin undergo three stages and possess a trilinear stress-strain relationship, which is why all cells are filled in for those coupons.

Table 5. Overview of key load-displacement phases for sandwich beams composed of partial bio-resin PET FRP facings and R-PET honeycomb core.

Set #	Specimen ID	K_1 (N/mm)	δ_u (mm)	F_u (N)
1	BE-ft1-S-1	236.0	8.0	1674.6
	BE-ft1-S-2	193.2	9.7	1653.6
	BE-ft1-S-3	203.3	7.9	1552.7
	Average	**210.8**	**8.5**	**1627.0**
	SD	**22.3**	**1.0**	**65.2**
2	BE-ft2-S-1	304.8	10.0	2270.0
	BE-ft2-S-2	347.7	15.5	2405.0
	BE-ft2-S-3	303.0	12.3	2593.0
	Average	**318.5**	**12.6**	**2422.7**
	SD	**25.3**	**2.8**	**162.0**
3	BE-ft3-S-1	503.8	11.2	3277.8
	BE-ft3-S-2	461.3	12.1	3908.4
	BE-ft3-S-3	516.5	8.2	2941.9
	Average	**493.9**	**10.5**	**3376.0**
	SD	**28.9**	**2.0**	**490.7**
4	BE-ft1-W-1	176.1	12.5	1518.7
	BE-ft1-W-2	208.0	6.9	1128.9
	BE-ft1-W-3	202.8	11.1	1298.8
	Average	**195.6**	**10.2**	**1315.5**
	SD	**17.1**	**2.9**	**195.4**
5	BE-ft2-W-1	269.4	7.3	1272.8
	BE-ft2-W-2	305.9	18.1	1481.7
	BE-ft2-W-3	300.3	13.1	1629.7
	Average	**291.9**	**12.8**	**1461.4**
	SD	**19.7**	**5.4**	**179.3**
6	BE-ft3-W-1	488.4	9.5	2602.1
	BE-ft3-W-2	522.3	17.2	2659.1
	BE-ft3-W-3	438.7	15.9	1864.5
	Average	**483.1**	**14.2**	**2375.2**
	SD	**42.0**	**4.1**	**443.2**

Table 6. Overview of key load-displacement phases for sandwich beams composed of synthetic resin PET FRP facings and R-PET honeycomb core.

Set #	Specimen ID	K_1 (N/mm)	δ_u (mm/mm)	F_u (MPa)
7	E-ft1-S-1	176.2	18.6	1351.8
	E-ft1-S-2	265.2	19.3	1652.6
	E-ft1-S-3	218.7	16.0	1264.8
	Average	**220.0**	**18.0**	**1423.1**
	SD	**44.5**	**1.7**	**203.5**
8	E-ft1-W-1	201.1	15.7	1437.8
	E-ft1-W-2	220.5	22.8	1840.5
	E-ft1-W-3	220.1	9.1	1204.9
	E-ft1-W-4	193.2	20.1	1599.7
	Average	**208.7**	**16.9**	**1520.7**
	SD	**13.7**	**6.0**	**267.8**

Table 7. Overview of key load-displacement phases for sandwich beams composed of bio-resin PET FRP facings and R-PET honeycomb core.

Set #	Specimen ID	K_1 (N/mm)	δ_u (mm/mm)	F_u (MPa)
9	B-ft1-S-1	190.1	26.6	1608.7
	B-ft1-S-2	185.5	24.8	1367.8
	B-ft1-S-3	181.6	27.3	1464.7
	Average	185.8	26.2	1480.4
	SD	4.3	1.2	121.2
10	B-ft1-W-1	193.0	4.8	696.2
	B-ft1-W-2	192.6	13.6	1035.0
	B-ft1-W-3	192.6	5.9	778.0
	Average	192.7	8.1	836.4
	SD	0.2	4.8	176.8

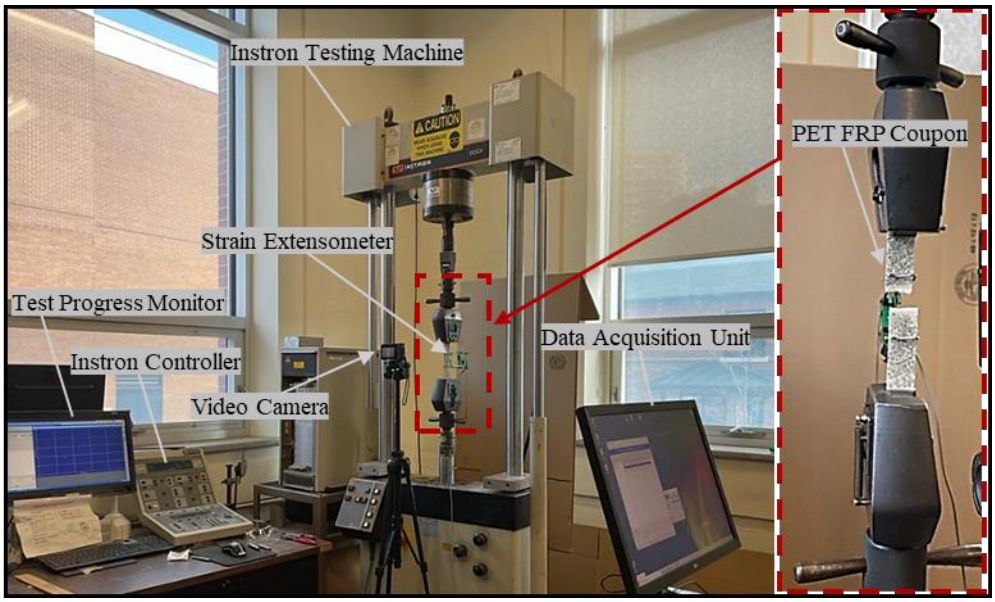

Figure 1. Uniaxial testing apparatus for PET FRP coupons.

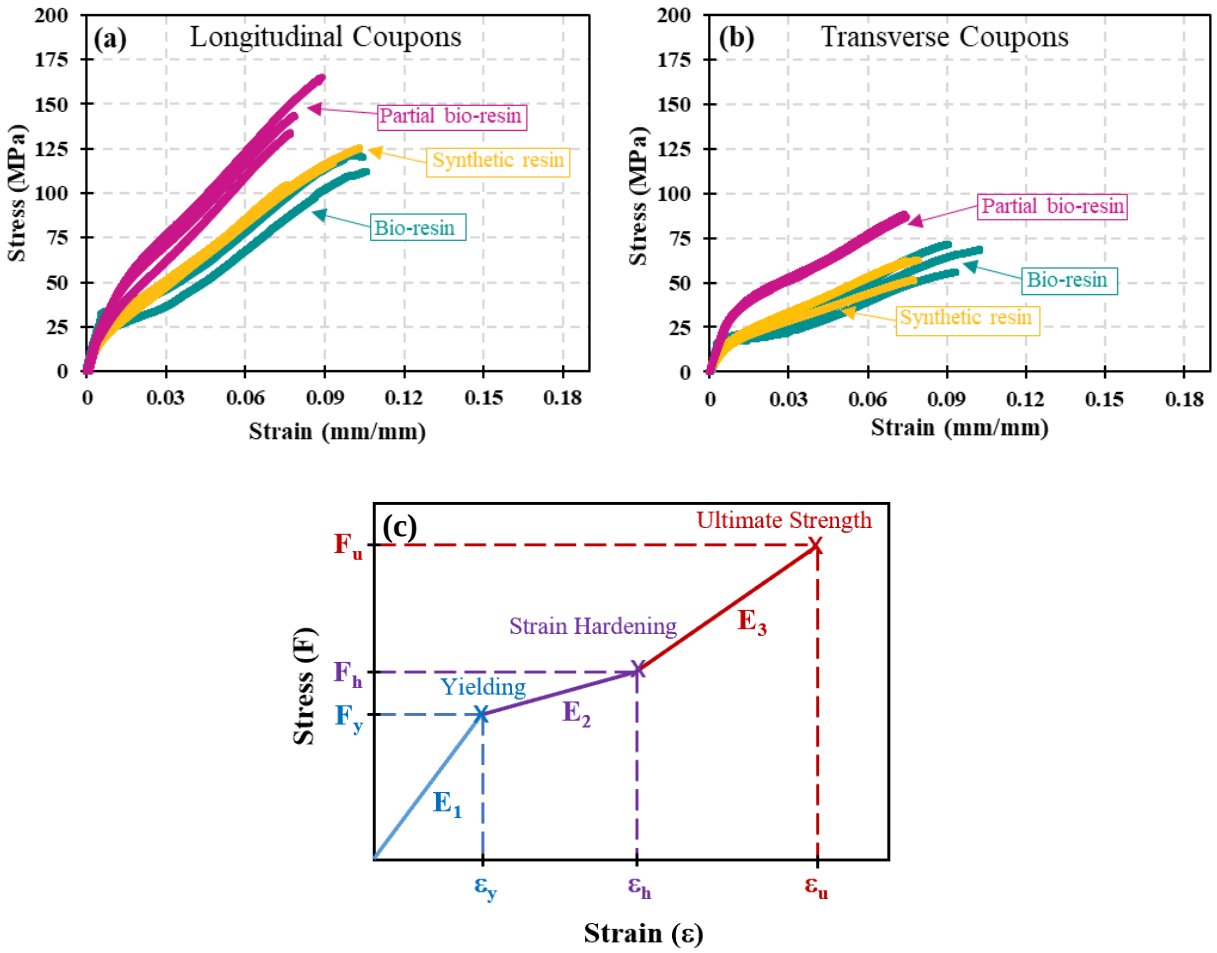

Figure 2. Stress-strain plots of PET FRP coupons in (a) longitudinal orientation; (b) transverse orientation; and (c) schematic of the stress-strain curve illustrating the tri-linear trend, with labeled regions indicating the yielding, strain-hardening, and ultimate strength stages.

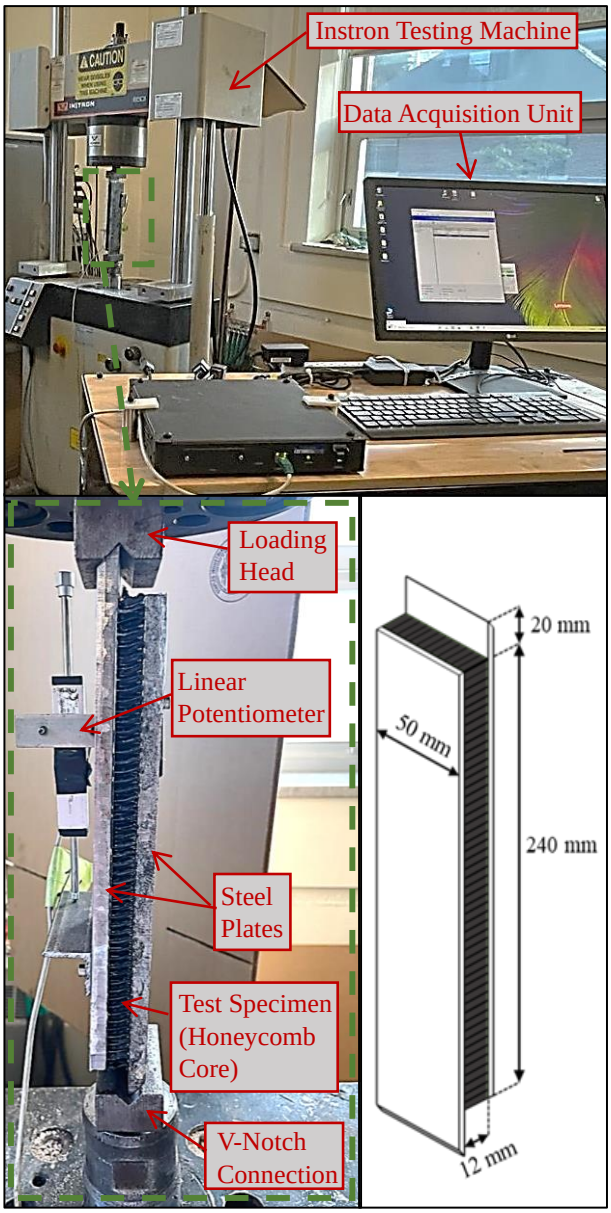

Figure 3. Apparatus for shear testing of R-PET honeycomb specimens.

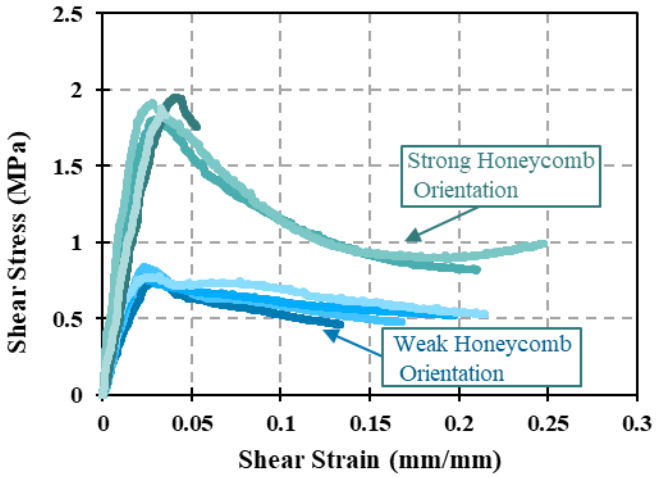

Figure 4. Shear stress-strain relation of R-PET honeycomb.

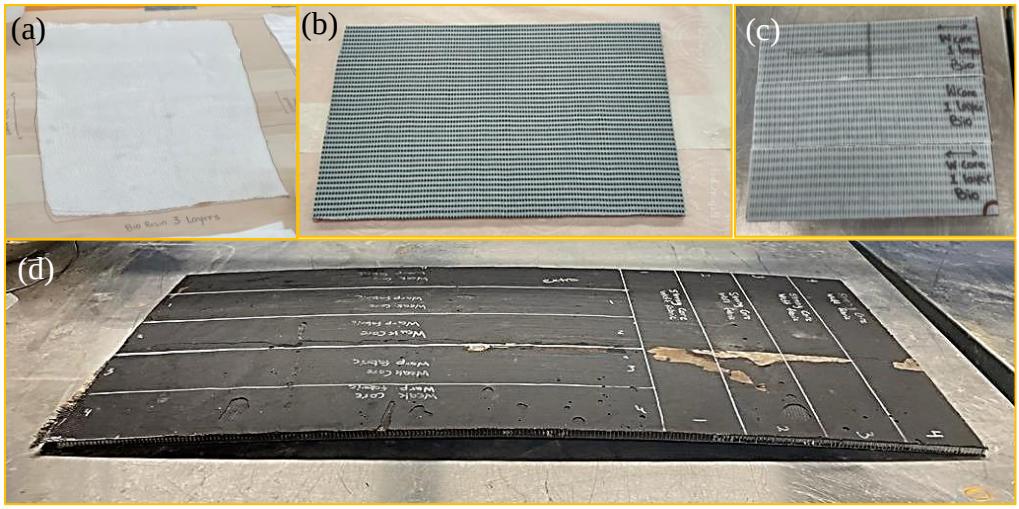

Figure 5. Selected stages in sandwich beam fabrication: (a) application of first PET fabric layer; (b) positioning of honeycomb core on first facing component; (c) cut beams from sandwich panel; (d) side view of moisture-curled bio-resin sandwich panel.

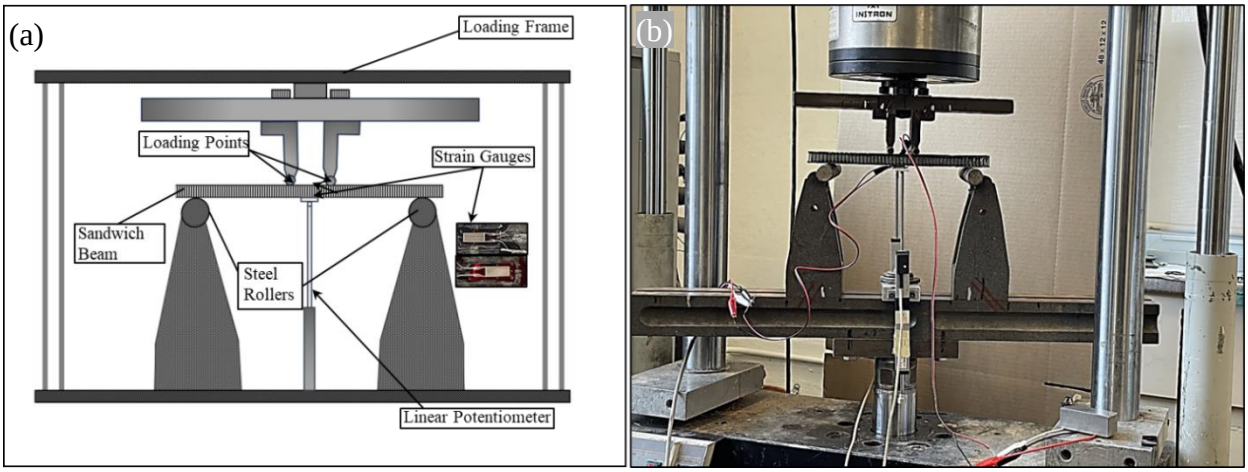

Figure 6. Four-point bending apparatus: (a) schematic overview; (b) photo of a sandwich beam specimen, measuring a total of 250 mm in length, which includes a 200 mm unsupported central span and 25 mm overhangs on each end.

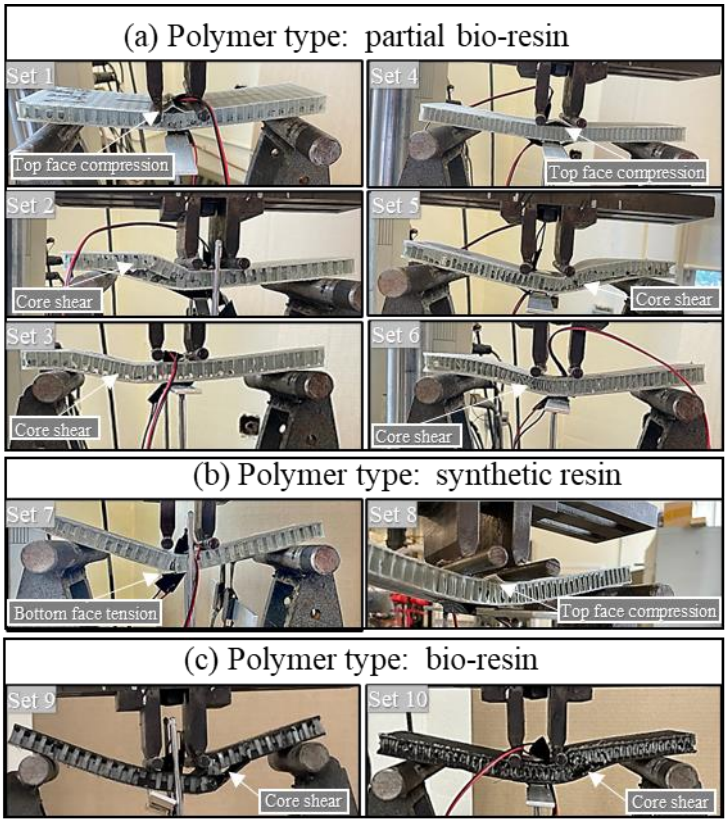

Figure 7. Categorization of failure modes observed in sandwich beam sets: (a) Sets 1-6: Set 1 - Tensile face rupture, Sets 2-3 and 5-6 - Core shear failure, Set 4 - Top face rupture; (b) Sets 7-8: Set 7 - Bottom face rupture, Set 8 - Top face rupture; (c) Sets 9-10: Both demonstrating core shear failure.

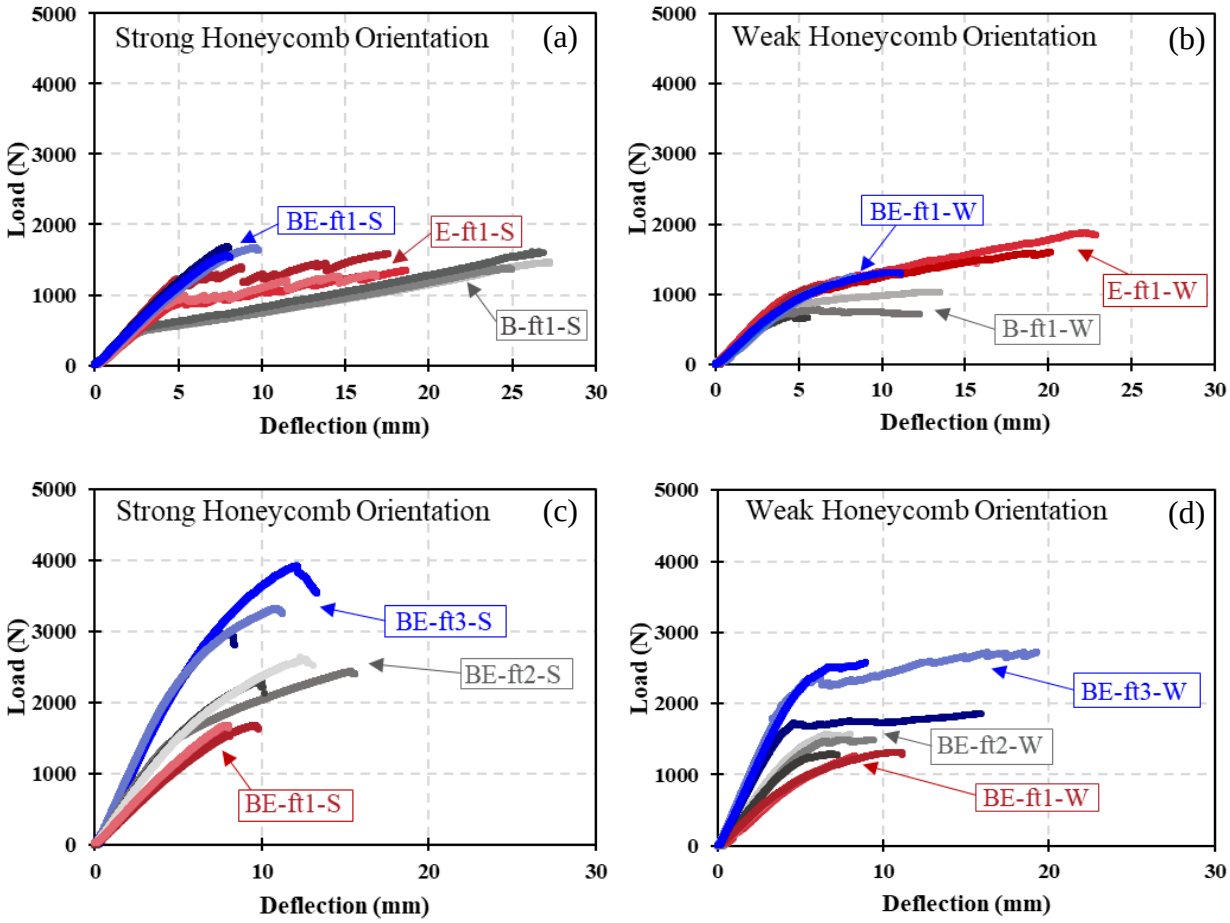

Figure 8. Load vs. midspan deflection curves for various sandwich beam configurations: (a) strongly oriented R-PET core with varied polymer matrices; (b) weakly oriented R-PET core with varied polymer matrices; (c) strongly oriented R-PET core, partial bio-resin with diverse PET FRP thicknesses; (d) weakly oriented R-PET core, partial bio-resin matrices with diverse PET FRP thicknesses.

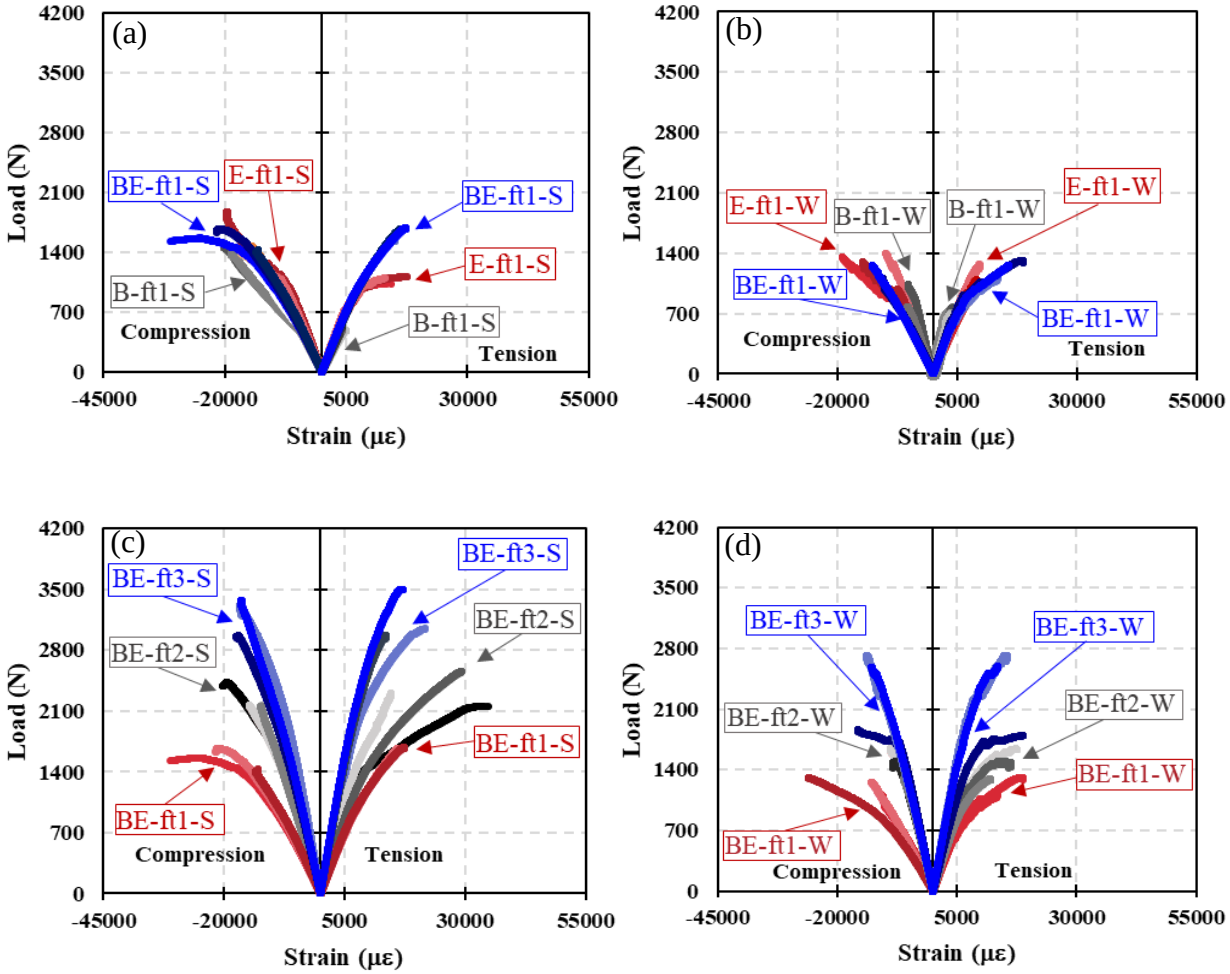

Figure 9. Load vs. strain curves for various sandwich beam configurations: (a) strongly oriented R-PET core with varied polymer matrices; (b) weakly oriented R-PET core with varied polymer matrices; (c) strongly oriented R-PET core, partial bio-resin matrices with diverse PET FRP thicknesses; (d) weakly oriented R-PET core, partial bio-resin matrices with diverse PET FRP thicknesses.

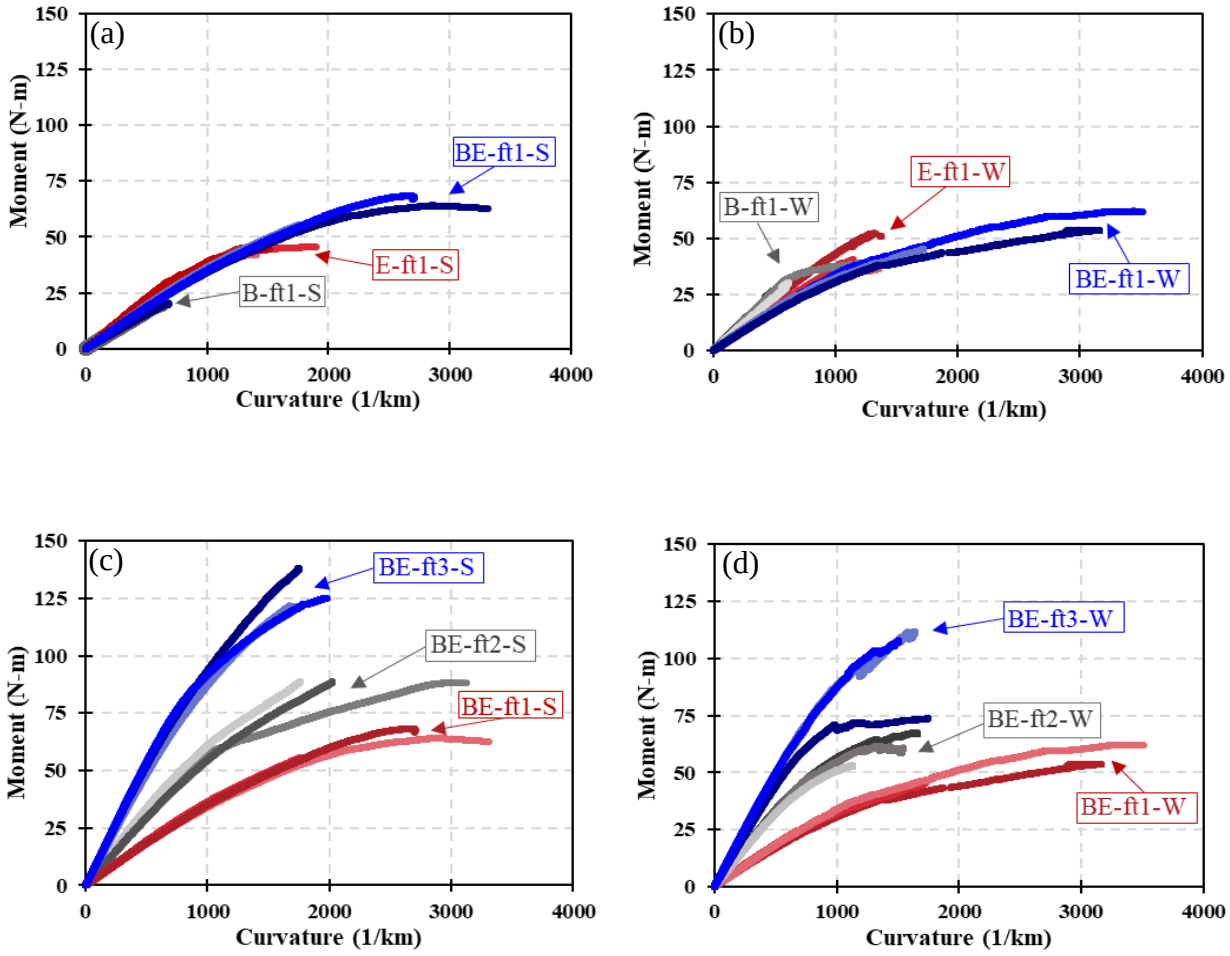

Figure 1. Moment vs. curvature curves for various sandwich beam configurations: (a) strongly oriented R-PET core with varied polymer matrices; (b) weakly oriented R-PET core with varied polymer matrices; (c) strongly oriented R-PET core, partial bio-resin matrices with diverse PET FRP thicknesses; (d) weakly oriented R-PET core, partial bio-resin matrices with diverse PET FRP thicknesses.

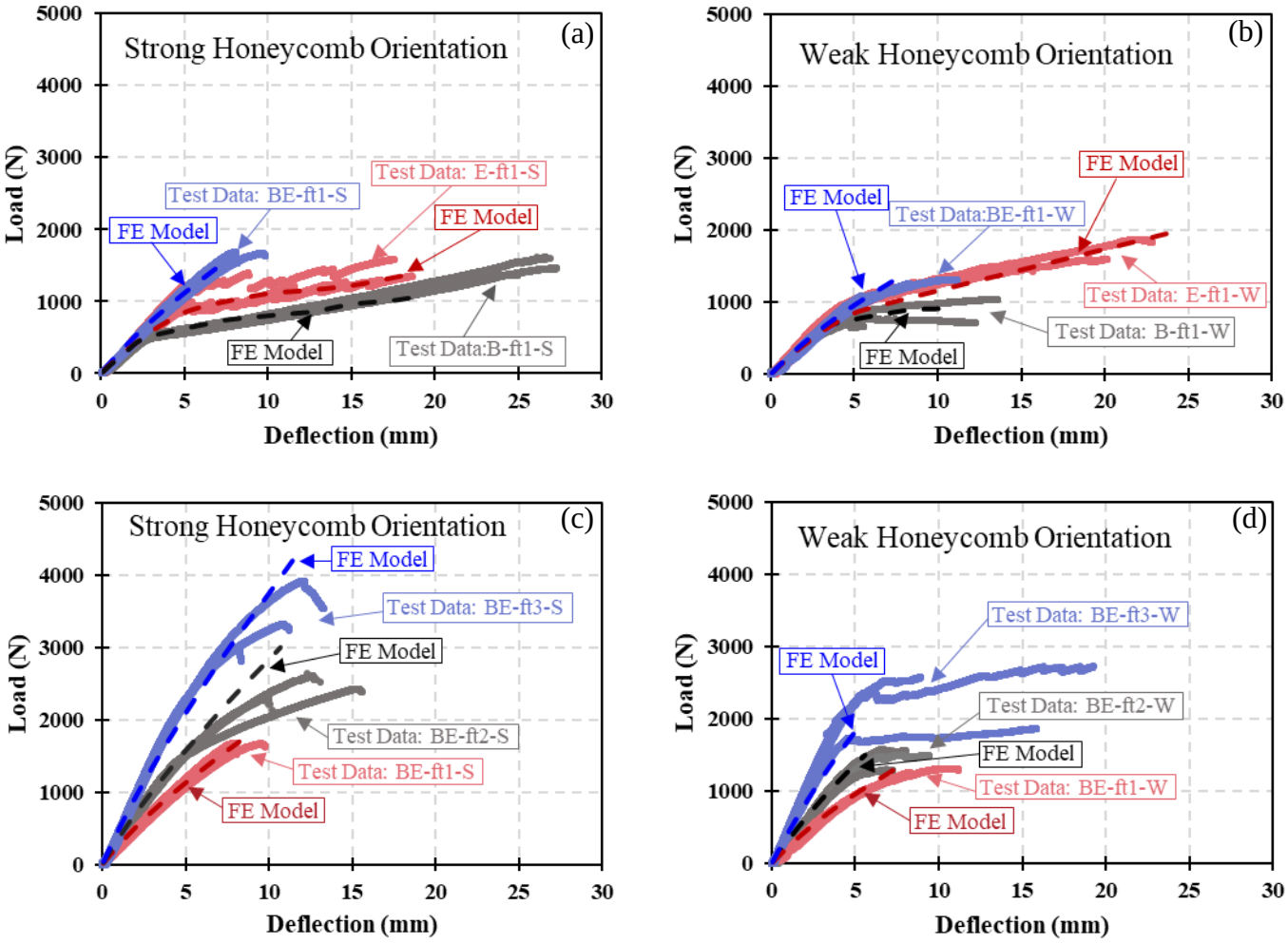

Figure 11. Load vs. deflection curves comparing FE simulation results (dashed lines) and experimental testing data (solid lines) for various sandwich beam configurations: (a) strongly oriented R-PET core with varied polymer matrices; (b) weakly oriented R-PET core with varied polymer matrices; (c) strongly oriented R-PET core, partial bio-resin matrices with diverse PET FRP thicknesses; (d) weakly oriented R-PET core, partial bio-resin matrices with diverse PET FRP thicknesses.